JOURNAL OF MATERIALS SCIENCE 37 (2002) 4145–4153

Electrophoretic deposition infiltration of 2-D metal fibre-reinforced cordierite matrix composites of tubular shape

C. KAYA*, F. KAYA
Interdisciplinary Research Centre (IRC) in Materials Processing and School of Metallurgy and Materials, The University of Birmingham, Edgbaston, Birmingham, B15 2TT, UK
E-mail: c.kaya@bham.ac.uk

A. R. BOCCACCINI
Department of Materials, Imperial College of Science, Technology and Medicine, Prince Consort Road, London SW7 2BP, UK

Stainless steel (316L) fibre mats shaped into tubular geometry were used to reinforce cordierite. The ductile phase-reinforced cordierite matrix composites were manufactured by using electrophoretic deposition (EPD) and pressureless sintering. An EPD cell suitable for the fabrication of tubular composites was designed. The relevant process parameters required to infiltrate the fibre mats with nanosized cordierite powders and to obtain homogeneous electrophoretic cordierite deposits on the inner and outer surfaces of the fibrous substrate were optimised. EPD experiments were conducted under constant voltage conditions (5 V dc) with varying deposition times. The sintered composites having internal and external deposit thickness of about 1 mm were free of surface cracks when a deposition time of 2.5 min was used. The developed metal fibre reinforced cordierite composites may constitute a promising alternative for manufacturing damage-tolerant tubular components for applications at intermediate-temperatures (up to ~900°C).
© *2002 Kluwer Academic Publishers*

1. Introduction

Cordierite ($2MgO\text{-}2Al_2O_3\text{-}5SiO_2$) and cordierite-based glass-ceramics are of interest for microelectronic applications, such as multilayered substrate materials, because of their low dielectric constant (4–6 at 1 MHz), low dielectric loss [1], relatively low coefficient of thermal expansion ($1\text{–}2 \times 10^{-6}/°C$ from 25 to 1000°C) and high volume resistivities ($>10^4\ \Omega$ cm) [2]. Due to its low thermal expansion coefficient and consequently high thermal shock resistance, cordierite has been also considered to be a candidate material for structural applications involving high temperatures [3]. However, the use of cordierite in load-bearing applications remains limited due to its relatively poor mechanical properties (flexural strength <200 MPa and fracture toughness $<2\ MPa \cdot m^{1/2}$).

The mechanical properties of cordierite can be enhanced by forming a composite material, i.e., by incorporating particles, whiskers, platelets or fibres into the cordierite matrix [4, 5]. In the case of fibre reinforcement mostly ceramic fibres, e.g., SiC-based, have been used to fabricate cordierite composites [6].

Due to the lack of availability of suitable low-diameter and temperature-resistant metallic fibres, the development of metal fibre reinforced ceramic matrix composites has not been extensively considered in the past. This situation however is changing in recent years due to the increasing commercial availability of fine metallic fibres and fibre fabrics with potential to be used as reinforcement in brittle matrices [7]. Thus, research on continuous fibre reinforced glasses and ceramics, including 2-dimensional reinforced composites, has gained some renewed impulse in the last few years [7–13].

Some advantages arise when using metallic fibres to reinforce brittle matrices. These include an increased resistance to damage during composite processing due to the intrinsic ductility of metallic fibres and the possibility of exploiting their plastic deformation for composite toughness enhancement [7].

Fabrication of ceramic composites with 2-dimensional (2-D) and 3-dimensional (3-D) fibre reinforcement is a challenge because it is difficult to achieve complete infiltration of the matrix material into the fibre tows, where the openings are of the order of 100 nm [8]. Thus, to obtain the desired properties through a controlled composite microstructure, it is crucial to develop reliable processing techniques to fully infiltrate the tight spaces of 2-D and 3-D fibre

*Also affiliated with Metallurgical and Materials Engineering Department, Yildiz Technical University, Istanbul, Turkey.

preforms. The fabrication technique should be also simple and cost-effective.

Recently, preliminary studies have demonstrated the feasibility of infiltrating metallic woven fibre mats with very fine boehmite sols (50 nm) and silica sols (40 nm) using electrophoretic deposition (EPD) [8–10]. EPD relies on the presence of small charged particles in a liquid, i.e., a sol, which, on the application of an electric field, will move to and deposit on an oppositely charged electrode [14]. This technique requires only low-cost equipment and offers new possibilities for the design of ceramics monoliths and films, fibre-reinforced composites and graded materials with uniform microstructures [14–19]. However, application of the EPD technique for the manufacturing of fibre-reinforced composites has been limited so far to the fabrication of simple planar and prismatic shape components [17].

The objective of the present work is to explore the possibility of using the EPD technique for the fabrication of metal fibre reinforced cordierite matrix composites, focusing on the manufacture of components of non-planar shape (three-dimensional components). In particular, a previously developed EPD cell [20] was modified in order to produce composite tubes using a single step forming process. Microstructural characterisation of the composite was carried out.

2. Experimental work

2.1. Materials

High purity stoichiometric α-cordierite ($2MgO \cdot 2Al_2O_3 \cdot 5SiO_2$) powder (Baikowski Chemie, France) was chosen as matrix material. As-received powders were first dispersed in distilled water at a pH value of 3 and then ball-milled in a plastic container for 2 days using high purity TZP (tetragonal zirconia polycrystals) balls as milling media. The ball-milled cordierite suspension was then vacuum filtered using a filter paper having 200 nm pore size. The powders that passed through the filter paper were collected for particle size analysis. Powders having an average particle size of 120 nm were re-dispersed in distilled water with the addition of 0.5 wt% B_2O_3 powder. B_2O_3 was added to increase the sinterability of the cordierite powder. Ultrasonic agitation was then employed at 15 kHz for 8 h for further dispersion of the particle agglomerates that might have been present. Kinetically stable and well-dispersed suspensions were obtained at a pH value of 3. At this pH value, cordierite powders had positive surface charge, as determined by surface charge analyser (Delsa 440 Analyser). The solids-loading of the suspension was kept at 20 wt%. This suspension was suitable for the EPD experiments as explained below.

The metallic reinforcement used in this work was made of stainless steel fibres (14 μm in diameter) laid-up in a 3D labyrinth architecture and sintered to form a filter felt, which is commercially available (Bekipor® ST, Bekaert Fibre Technologies, Belgium). This particular fibre preform was chosen on the basis of its suitability to be infiltrated by nanosized particles using EPD, as shown below. This grade of stainless steel fibre (316 L) can be used up to 900°C in an oxidising atmosphere [9] and its thermal expansion coefficient (20–700°C) is $16.8 \times 10^{-6}/°C$. Due to the relatively low thermal capability and oxidation resistance of the metallic fibre used, it must be ensured that the cordierite material used for the matrix be consolidated at temperatures $<\sim$900°C.

2.2. Composite fabrication: electrophoretic deposition and sintering

The flow chart for the manufacturing of tube shaped composites is schematically shown in Fig. 1. The plain metallic fiber mat was formed into a tubular shape of diameter 45 mm. The EPD cell used is schematically shown in Fig. 2. This EPD cell was constructed on the basis of a previously developed EPD technique [20]. Both positive electrodes, i.e., the central rod electrode and the cylindrical electrode surrounding the tubular fiber mat were made of stainless steel. The distance between the deposition electrode (fiber mat) and both

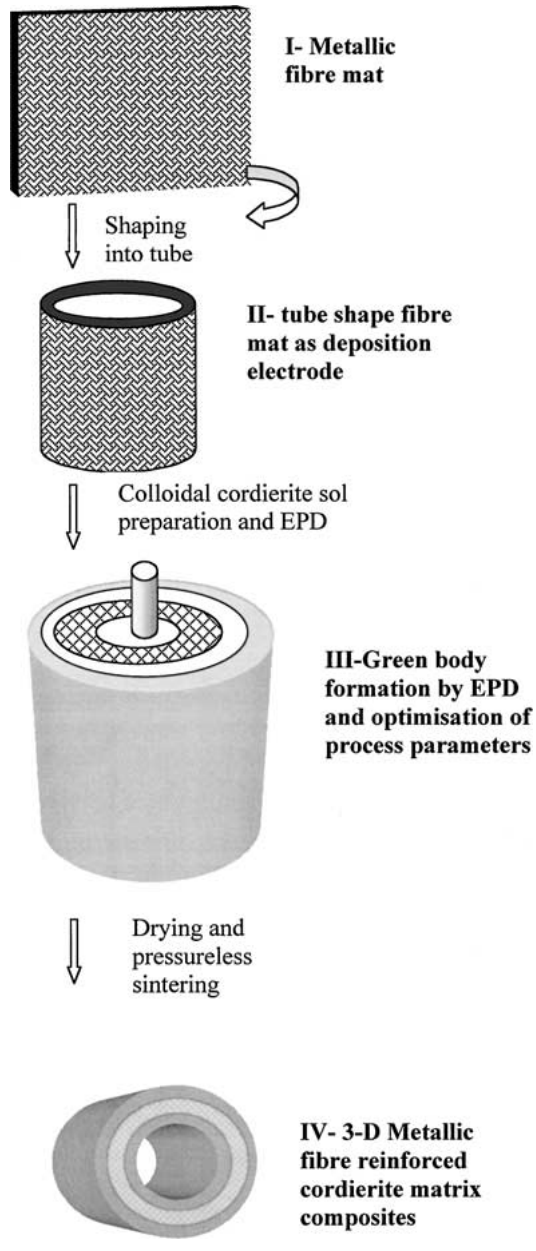

Figure 1 Flow chart showing the steps for the fabrication of 3-D tubular shape ceramic composites.

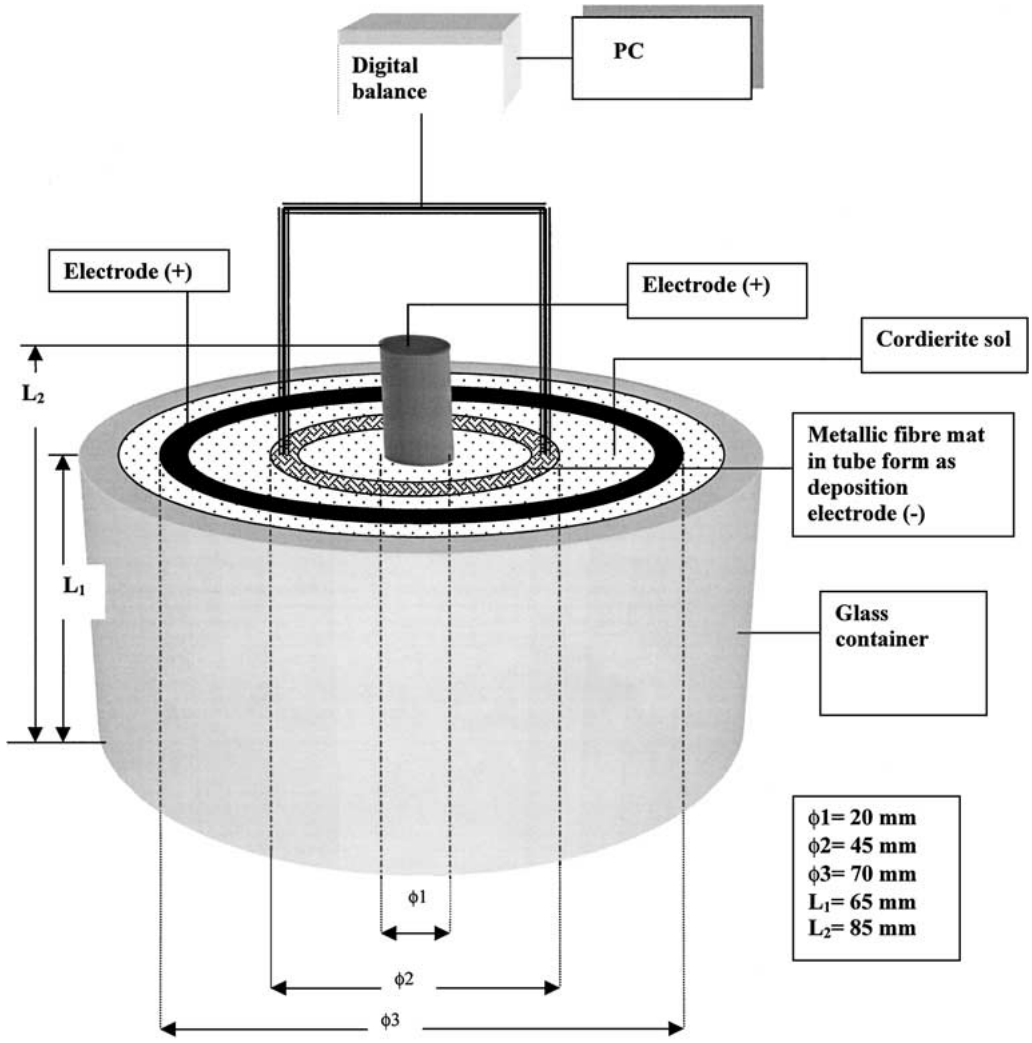

Figure 2 Schematic representation of the EPD cell used to produce stainless steel fiber-reinforced cordierite matrix composites of tubular shape.

positive electrodes was adjusted to be 12.5 mm. All experiments were carried out under constant voltage conditions (5 V d.c.) and the deposition time was varied to optimise the deposited ceramic thickness in terms of avoidance of microcracking development and final fibre volume fraction. The applied voltage was kept constant at 5 V d.c. because using a higher voltage would lead to decomposition of water in the suspension and thus to the evolution and entrapment of bubbles (porosity) into the green body compact.

The EPD-formed green compacts were first kept in a humidity chamber (80% relative humidity) for 1 day, then in a second chamber (50–60% relative humidity) for another day and subsequently they were exposed to normal air for another day. This careful drying process was necessary to avoid possible crack formation due to the rapid removal of the water from the green body. The dried samples were then pressureless sintered in air at 900°C for 2 h using 5°C/min heating and cooling rates.

2.3. Microstructural observations

High-resolution field emission gun scanning electron microscopy (FEG-SEM, Hitachi S-4000, Japan), which achieves resolutions of 2–5 nm at 30 kV, was used to observe the as-received and as-filtrated cordierite powder. The microscope was also used to investigate the structure of the metallic fibre mats and to examine the quality of the electrodeposited material. This was investigated in terms of extent and homogeneity of deposition, deposit thickness and degree of densification and microcracking formation after sintering. For microstructural observations, the green samples were embedded in resin using a vacuum impregnation equipment but not polished in order to avoid damage (e.g., spalling) of the ceramic deposit. Sintered samples were polished using a 3 μm diamond paste.

3. Results and discussion

SEM microstructures showing the as-received and vacuum-filtered α-cordierite powders are shown in Fig. 3a and b, respectively. The as-received powders are in a heavily agglomerated state and show a wide range of particle sizes, as shown in Fig. 3a, whereas the vacuum-filtered powder exhibits a homogeneous dispersion and uniform particle size with an average diameter of 120 nm (Fig. 3b). The powder microstructure obtained after vacuum filtering is ideal for EPD as the particles are spherical and almost of the same diameter. The particles in suspension in the EPD cell have therefore similar mobility, meaning that they will move and deposit onto the deposition electrode with the same speed.

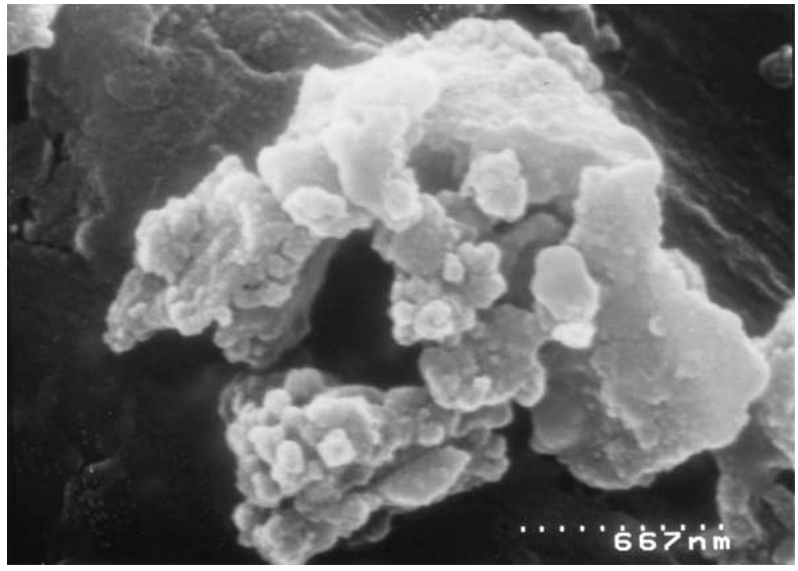

(a)

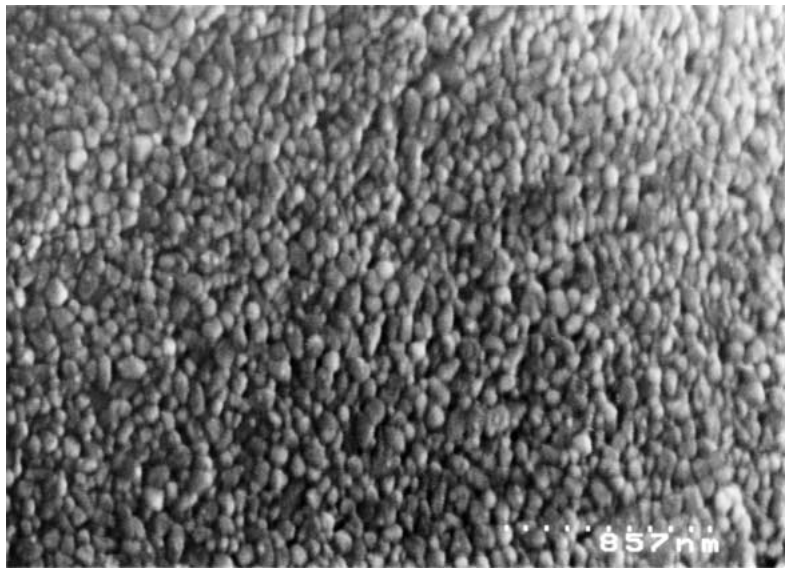

(b)

Figure 3 FEG-SEM micrographs showing: (a) as-received cordierite powders in highly agglomerated state and (b) agglomerate-free cordierite powder after ball-milling and vacuum filtration. Note in (b) the homogeneous particle size distribution with average particle size of about 120 nm.

The microstructure of the stainless steel (316 L) fibre mats used is shown in Fig. 4a and b at low and high magnifications, respectively. The SEM images demonstrate that individual fibers are continuous and multidirectional. The fibre preform shows also the ideal architecture to be infiltrated by nanosized powders using EPD, as the fibre openings are about 200 nm.

Cordierite nanoparticles in aqueous suspension at pH 3 will have an overall positive charge under the effect of an electric field. This charge is produced by the adsorption of H^+ ions, which in turn results in a double layer surrounding the particle. The applied electric field causes the positive and negative portions of this double layer to displace relative to each other and this in turn causes the particles to migrate towards and deposit on the tubular fibre mat acting as cathode (Fig. 2). FEG-SEM images indicating the green and sintered microstructures of EPD-formed stainless steel fibre-reinforced cordierite matrix composites are shown in Fig. 5a and b, respectively. These deposits were obtained using a voltage of 5V and a deposition time of 2.5 min. The green microstructure after drying shown in Fig. 5a confirms that the cordierite sol particles have been attracted to and deposited onto the tube-shape fibre mat, thus producing a green body composite compact. It is also seen that the dried microstructure contains no microcracks. The sintered microstructure (900°C for 2 h) indicates the dense nature of the cordierite matrix with no sintering flaws formed (Fig. 5b).

The thickness of individual layers in multilayered ceramic composite components is a critical parameter affecting the composite performance under mechanical and thermal loads [21]. Moreover deposit thickness is a limiting factor in relation to the possibility of producing crack-free green bodies, since the likelihood of microcracking development upon drying of ceramic deposits or gels strongly depends on their thickness [22].

In this work, special attention was given to control the thickness of the EPD-formed cordierite deposit by altering the deposition time. The thickness of the

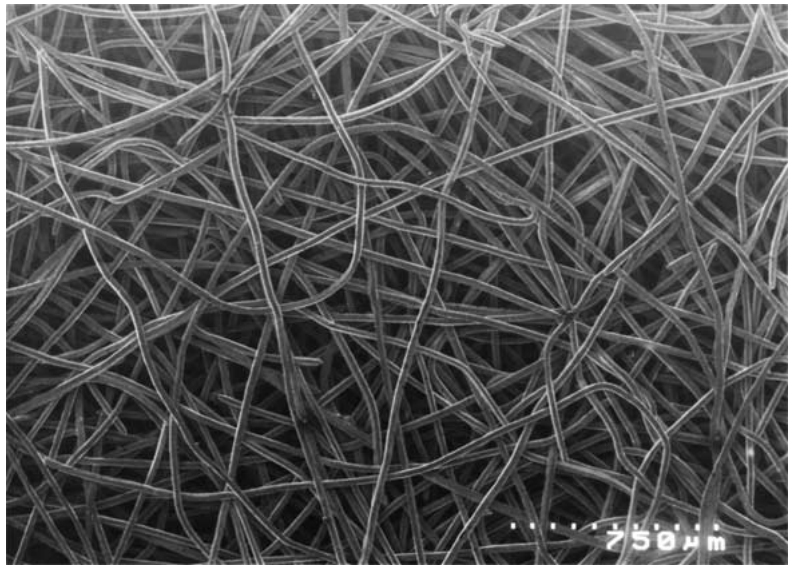

(a)

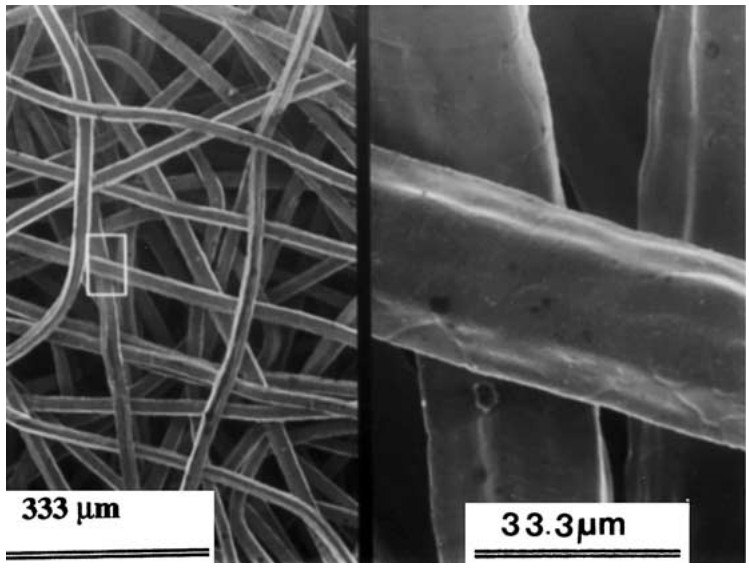

(b)

Figure 4 FEG-SEM micrographs of 316L stainless steel fibres showing: (a) the general 3-D labyrinth architecture suitable for EPD infiltration and (b) a detailed high-magnification image confirming individual fibre diameter to be 14 μm and fibre interspaces of ~200 nm.

TABLE I The effect of the deposition time during EPD, at a voltage of 5 V dc, on deposit thickness and microcracking development after drying

EPD time (Min.)	EPD deposit thickness (μm)	State of deposit surface
0.5	310	Crack free
1	540	Crack free
1.5	705	Crack free
2	920	Crack free
2.5	1010	Crack free
3	1060	Extensive cracks
3.5	1090	Extensive cracks
4	1105	Extensive cracks
4.5	1115	Extensive cracks

EPD-formed layer as a function of deposition time is given in Table I. A significant increase in deposit thickness was recorded for deposition times up to 2.5 min. As the deposition time is increased from 2.5 min to 4.5 min, only a limited increase in thickness is observed. In EPD experiments carried out under constant voltage conditions, such as in the present study, the current increases with time as the electrical resistance of the deposited layer continually increases. It has been shown that the deposition rate decreases with time as the potential difference across the layer decreases according to the following equation [23]:

$$\frac{\mathrm{d}n}{\mathrm{d}t} = \frac{NZ(V_{appl} - V_{film})}{D} \quad (1)$$

where n is the number of particles deposited per unit area, N is the particle density of the sol, Z is the electrophoretic mobility (which depends on: dielectric constant and viscosity of the liquid, a geometrical shape parameter and the zeta potential of the suspension), V_{appl} is the applied voltage, V_{film} is the potential across the deposited film and D is the separation between the electrodes. Under the EPD conditions used in this work (5 V d.c.), it is found that the ideal deposition time is 2.5 min, resulting in a deposit thickness of 1010 μm for the

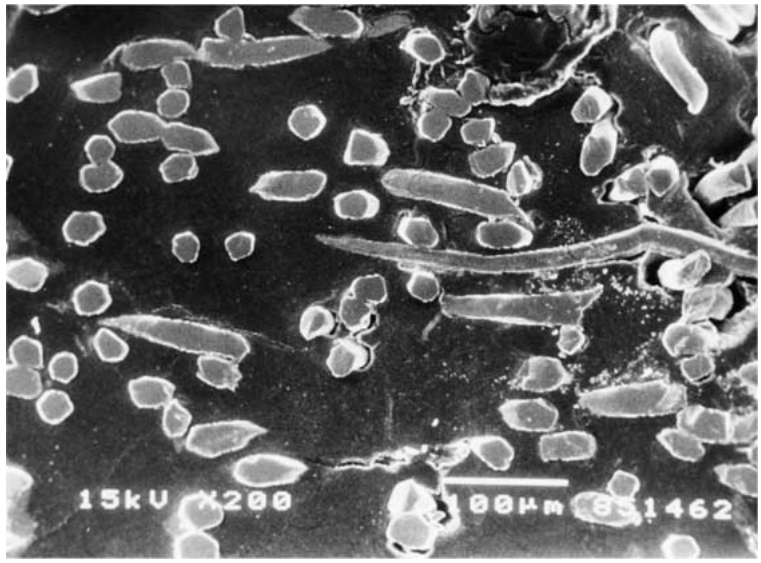

(a)

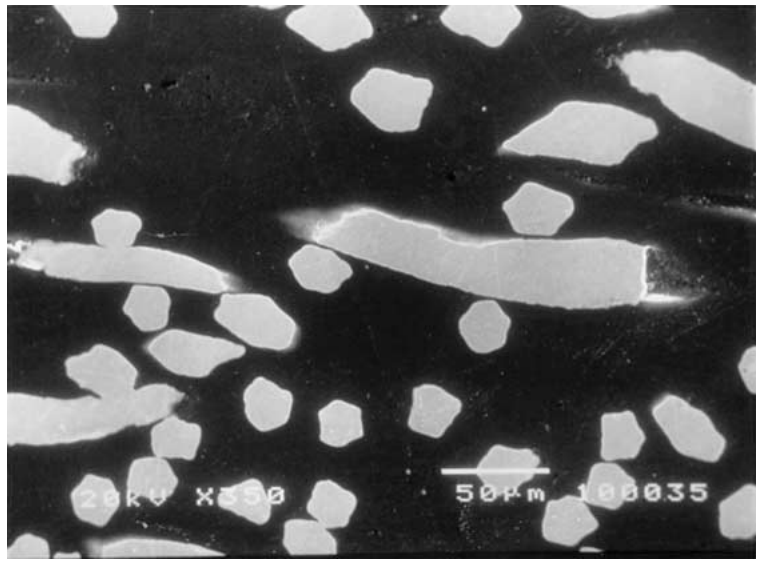

(b)

Figure 5 FEG-SEM micrographs of cordierite matrix composites showing: (a) green microstructure after drying and (b) sintered microstructure after sintering at 900°C for 2 hr. Samples were produced by EPD using an applied voltage of 5 V dc and a deposition time of 2.5 min. Note the complete infiltration of cordierite powder and the crack-free microstructure in both the green and sintered stages.

particular fibre architecture and cordierite powder used. Optimal EPD conditions are strongly dependent on the ceramic suspension and type of fibre used. In a recent work on EPD using woven fibre mats of the same stainless steel 316L used here but with boehmite nanoparticles, the optimised voltage and deposition time were 4 V and 2 min, respectively [24].

The microstructure of a sintered composite sample produced using a deposition time of 4.5 min is shown in Fig. 6. The microstructures of deposits taken from the internal and external surfaces of the tubular composite are shown in Fig. 6a and b, respectively. Both pictures show the presence of microcracks, which are thought to develop during the drying of the EPD deposits and which are not "healed" during sintering. However, the extent of microcracking formed in the internal surface of the tubular composite (Fig. 6a) is higher than that created at the external surface (Fig. 6b). The cross-sectional SEM image of the same sample confirms that the cracks, created either on the inner or outer surfaces of the tubular composite, propagate in the cordierite matrix through the thickness of the composite, as shown in Fig. 7. On the other hand, a sintered sample produced using a deposition time of 2.5 min has a deposit thickness of 1010 μm (see also Table I) and contains no cracks, as shown in Fig. 5b. There are two main models published in the literature to account for the origin of drying cracks in ceramic deposits [22]. According to the most widely accepted approach, during drying, crack formation occurs due to differential shrinkage of the ceramic matrix network generating tensile stresses at the surface and causing catastrophic growth of microscopic flaws. Drying produces a pressure gradient in the liquid phase of the matrix because as liquid evaporates from the surface, more liquid diffuses from the centre of the matrix to the surface to replace it. The external region of the matrix thus shrinks faster than the interior as a result of this pressure gradient, producing tensile

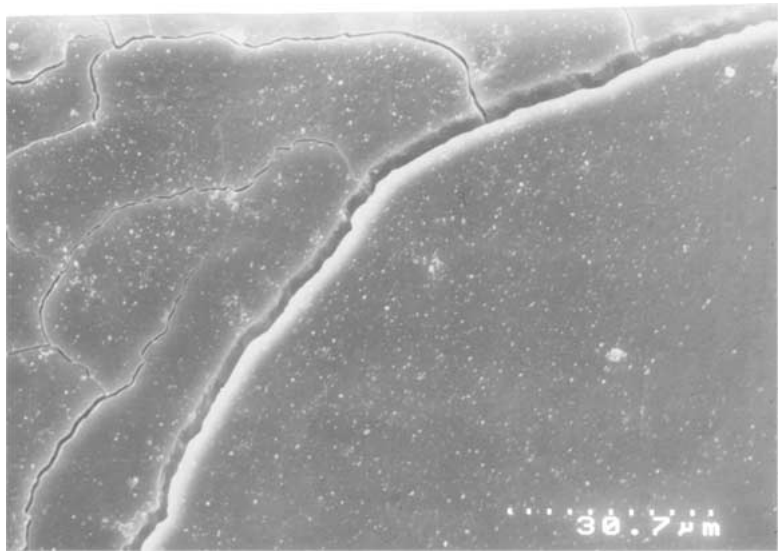

(a)

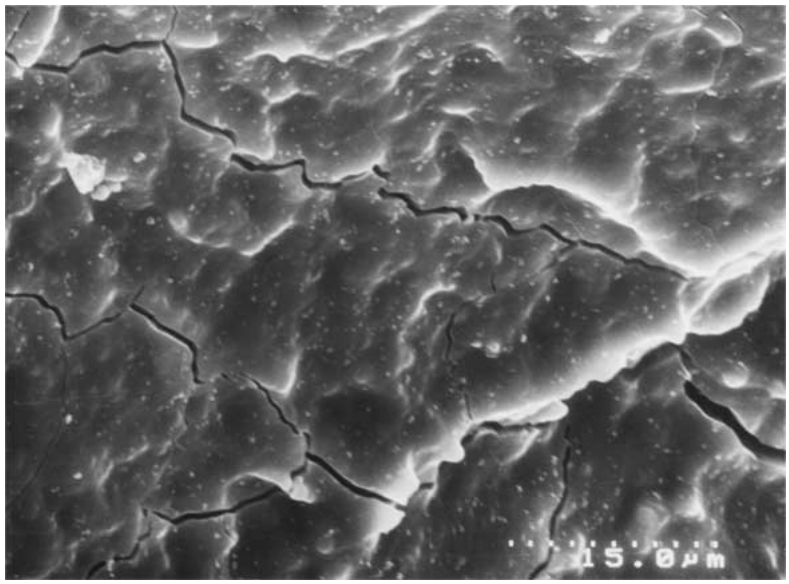

(b)

Figure 6 FEG-SEM micrographs of a sintered composite sample produced by EPD using an applied voltage of 5 V dc and a deposition time of 4.5 min, showing extensive microcracking: (a) at the inner and (b) outer surfaces of the tubular composite.

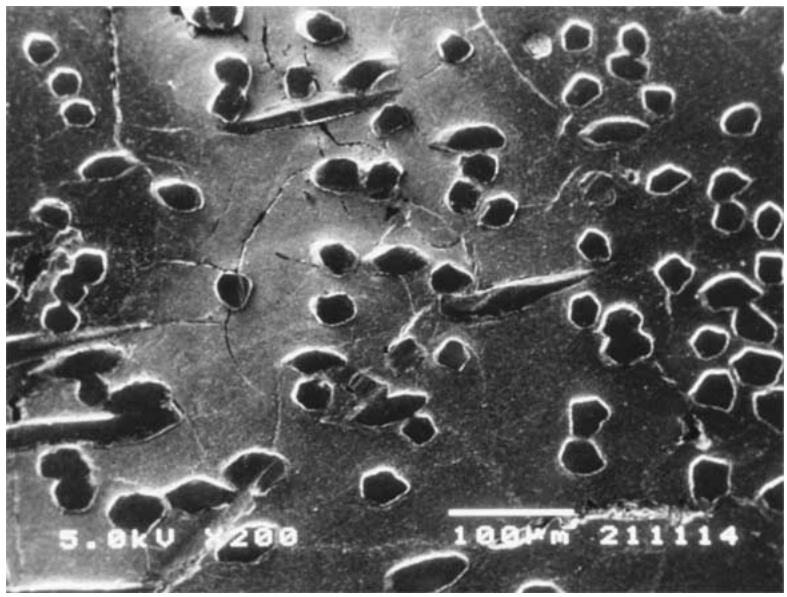

Figure 7 FEG-SEM micrograph of the cross section of a sintered composite sample showing that the cracks created on the inner and outer surfaces of the tube progress through the cordierite matrix.

stresses throughout the matrix network that are larger at the exterior. Contraction is inhibited by the slower contraction of the internal region where liquid tension is lower. The network at the interior is stretched, this promoting cracking by growth of pre-existing microscopic flaws.

It can be concluded from the results presented in Table I and in Figs 5–7 that the maximum deposit thickness exhibiting a crack-free microstructure is about 1 mm for the fibre mat type and cordierite powder used in this work. As mentioned above, the nature of the cracks created at the inside and outside surfaces of the tube are very different, as shown in Fig. 6a and b. The crack configuration formed in the internal surface consists of a main wide (6 μm in width) crack with smaller curved cracks intersecting the main crack, as shown in Fig.6a, with an inter-crack spacing of about 250 μm. The cracks formed at the outer surface of the tube composite (Fig. 6b) show a different morphology. It is seen that there is one curved main crack (2 μm in width), which propagates on the surface with an inter-crack spacing of about 50 μm. In order to eliminate the microcrack formation, if a deposit thickness higher than 1 mm is required, alternative drying systems with even slower liquid extraction rate, such as freeze drying, should be examined.

It should be mentioned that two other sources for microcracking may exist during manufacturing of the composites: (i) during sintering due to constrained densification of the cordierite matrix as it shrinks in the presence of a rigid (i.e., non-sintering) fibre perform, and ii) upon cooling from the sintering to room temperature due to the different thermal expansion characteristics of the matrix and fibres. Considering the result that for ceramic deposit thickness $<\sim$1000 μm no microcracking was observed, both before and after sintering, it was assumed here that all microcracks originated during the drying stage in deposits of large thickness, as mentioned above. The crack pattern shown in Fig. 7, however, may well be a combination of both "non-healed" drying microcracks and cracks developed due to both constrained sintering shrinkage and thermal expansion mismatch stresses.

It must be finally pointed out that densification of a stoichiometric crystalline cordierite powder compact is a difficult task [2]. Sintering aids, such as B_2O_3, P_2O_5 or lead borosilcate glass are usually added to reduce the viscosity at a given temperature and thus to increase the sinterability of cordierite powders [2, 25]. The approach followed here, addition of 0.5 wt% B_2O_3 to the starting cordierite powder, allowed sufficient densification of the cordierite matrix at a temperature of 900°C, achieving porosities $<\sim$5%.

An alternative approach, which does not involve the addition of sintering aids, is the "glass-ceramic route" [26]. In this method, amorphous powders of cordierite composition are used and densification takes place by exploiting the viscous flow of the glassy phase before crystallisation. The densified amorphous body is then submitted to a crystallisation heat-treatment to obtain the desired α-cordierite microstructure. The fabrication of cordierite composites reinforced by metallic fibre mats using this approach is the focus of current research.

4. Conclusions

Stainless steel fibre mats shaped into tubular geometry can be fully infiltrated and coated by nanosized cordierite powders (120 nm) using EPD under constant voltage conditions (5 V d.c). The optimised processing parameters used in this work resulted in the formation of dense deposited layers of about 1 mm in thickness with no drying or sintering cracks. However, if the deposit thickness is increased above this value by using longer deposition times, extensive microcracking occurs both on the inside and outside of the tubular composite. These microcracks were thought to be the result of stresses arising during the drying of the deposits. Microscopic observation revealed that microcracks, once formed in the green body, cannot be closed during the sintering stage. The experimental approach presented here shows a simple processing method to manufacture metal fibre reinforced cordierite matrix composites of non-planar shape. To the best of the authors' knowledge, this is the first report on the manufacturing of fibre reinforced cordierite matrix composites of tubular shape. Work is in progress to characterise the thermomechanical behaviour of the composites. They are expected to show non-catastrophic fracture behaviour as a result of energy dissipation by plastic deformation of the metallic fibres.

Acknowledgements

Very helpful discussions with Dr. K. C. Chan are acknowledged. The authors would like to thank Dr. R. de Bruyne, NV Bekaert S. A. (Belgium) for supplying the fibres. ARB acknowledges financial support of the Nuffield Foundation of London (UK) (Grant nr. NAL/00196/G).

References

1. B. MUSSLER and M. SHAFER, *Amer. Ceram. Soc. Bull.* **63** (1984) 705.
2. S. MEI, J. YANG and J. M. F. FERREIRA, *J. Europ. Ceram. Soc.* **21** (2001) 185.
3. M. PINERO, C. BARRERA-SOLANO, C. JIMENEZ-SOLIS, L. ESQUIVIAS and I. ZARZYCKI, *Ceram. Trans.* **74** (1997) 471.
4. I. WADSWORTH and R. STEWENS, *J. Mater. Sci.* **26** (1991) 6800.
5. W. SEMAR and W. PANNHORST, *Silicate Ind.* **3/4** (1991) 155.
6. M. C. LONG, R. E. MOORE, D. E. DAY, J. G. WESLING and R. BURNS, *Ceram. Eng. Sci. Proc.* **10**(9/10) (1989) 1231.
7. I. W. DONALD and B. L. METCALFE, *J. Mater. Sci.* **31** (1996) 1139.
8. A. R. BOCCCACCINI, J. OVENSTONE and P. A. TRUSTY, *Applied Composite Materials.* **4** (1997) 145.
9. A. R. BOCCACCINI and P. A. TRUSTY, *J. Mater. Sci.* **33** (1998) 933.
10. C. KAYA, A. R. BOCCACCINI and P. A. TRUSTY, *J. Eur. Ceram. Soc.* **19** (1999) 2859.
11. B. WIELAGE and M. PENNO, *VDI Berichte* **1151** (1995) 579.
12. B. METCALFE, I. DONALD and D. BRADLEY, in Proceedings of High Temperature Ceramic Matrix Composites, edited by R. Naslain, J. Lamon and D. Doumeingts (Woodhead Publ. Ltd., 1993) Vol. 1, p. 447.
13. A. E. RUDOVSKIJ, P. D. SARKISOV, A. A. IVASHIN and V. V. BUDOV, in "Ceramic- and Carbon-Matrix

Composites," edited by V. I. Trefilov (Chapman and Hall, London, 1995) p. 255.
14. P. SARKAR and P. S. NICHOLSON, *J. Amer. Ceram. Soc.* **79**(8) (1996) 1987.
15. O. VAN DER BIEST and L. VANDEPERRE, *Annual Rev. Mater. Sci.* **29** (1999) 327.
16. I. ZHITOMIRSKY and A. PETRIC, *J. Europ. Ceram. Soc.* **20** (2000) 2055.
17. A. R. BOCCACCINI, C. KAYA and K. K. CHAWLA, *Composites* A **32** (2001) 997.
18. C. KAYA, F. KAYA, A. R. BOCCACCINI and K. K. CHAWLA, *Acta Materialia* **49** (2001) 1189.
19. C. KAYA, A. R. BOCCACCINI and K. K. CHAWLA, *J. Amer. Ceram. Soc.* **83** (2000) 1885.
20. C. KAYA, PhD thesis, The University of Birmingham, UK, 1999.
21. W. A. CUTLER, F. W. ZOK, F. F. LANGE and P. G. CHARALAMBIDES, *J. Amer. Ceram. Soc.* **80** (1997) 3029.
22. C. J. BRINKER and G. W. SCHERER, "Sol-Gel Science: The Physics and Chemistry of Sol-gel Processing" (Academic Press, 1990).
23. Y. HIRATA, A. NISHIMOTO and Y. ISHIHARA, Nippon Seramikkusu Kyokai Gakujutsu Ronbunshi **99**(2) (1991) 108.
24. C. KAYA and A. R. BOCCACCINI, *J. Mater. Sci. Lett.* **20** (2001) 1465.
25. S.-L. FU, L.-S. CHEN and J. H. CHOU, *Ceram. Int.* **20** (1994) 67.
26. E. A. GIESS, C. F. GUERCI, G. F. WALKER and S. H. WEN, *J. Amer. Ceram. Soc.* **68** (1985) C-328.

Received 8 November 2001
and accepted 3 June 2002